Interaction between Light, Paper and Color Halftones: Challenges and Modelization Approaches

Roger David Hersch, Mathieu Hébert, Ecole Polytechnique Fédérale de Lausanne (EPFL), Switzerland

Abstract

We review the phenomena having an impact on the interaction between light, paper and color halftones. They comprise surface reflections and refractions at the air-paper interface, propagation of light within the paper, internal reflections at the paper-air interface, as well as ink spreading and trapping. We introduce basic notions from radiometry and optics, such as the definitions of radiant flux, irradiance, radiance, Lambert reflector, as well as collimated and diffuse light reflection and refraction. We then present classical spectral reflection models, their extension to multi-ink color halftones and the impact of different measuring devices (radiant detector, integrated sphere). Finally we briefly review ink spreading models and highlight the topics deserving further research.

Introduction

Accurate models of the interaction between light, paper and halftones may offer new ways of performing automatically the calibration of printing devices, e.g. upon change of the paper or of the ink cartridges. They may also help in regulating printing devices by ensuring that print parameters, such as the amount of deposited ink, remain constant, independently of the fact that the printer has just started printing or has been printing for a few hours. Finally, for printers capable of printing with many custom inks, spectral prediction models may help in computing the optimal combination of inks yielding a desired color.

Phenomena

Let us briefly review the main phenomena occurring when light hits a halftone image printed on paper (Fig. 1). Light incident on the print is partly reflected and partly refracted at the air-print interface. The amount of specularly reflected light and its angular distribution depends on the surface properties of the print and on the angular distribution of the incident light. The part of the incident light transmitted (refracted) into the print is the part that is not reflected at the print surface. The transmitted light is then further attenuated by the ink halftone layer and penetrates the paper bulk where it is scattered in all directions. Light scattering within the paper bulk induces both a lateral propagation of the light and a reflection from the paper bulk towards the ink halftone layer located beneath the print-air interface. There, it is attenuated by the ink halftones. At the print-air interface, part of the light is reflected towards the paper bulk and part of the light is transmitted (refracted) into the air. The part reflected for the second time by the paper bulk is again attenuated by the ink halftone and again reflected by the paper bulk and reemitted towards the print-air interface. The successive reflections between the paper bulk and the print-air interface yield the so-called *multiple internal reflections*.

At print time, there are further interactions between ink halftones and paper and between ink halftones and previously printed ink layers.

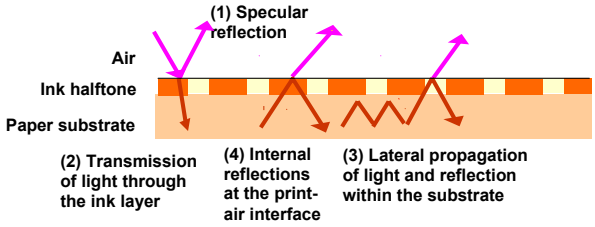

Figure 1. Phenomena contributing to the interaction between light, ink halftones and paper

A single ink halftone layer printed on paper generates an ink dot surface coverage which is generally larger than the corresponding nominal dot surface coverage value. The enlargement of the printed ink dot is called dot gain. The dot gain is the difference between effective dot surface coverage and nominal dot surface coverage. When an ink halftone is printed on top of another ink, e.g. a solid ink (100% surface coverage), the dot gain of the ink halftone is different than when it is printed alone on paper (Fig. 2). Dot gain therefore strongly depends on the superposition condition, i.e. on which other inks a given ink halftone is superposed. Note that the dot gain of an already printed ink halftone may be modified by a second ink printed on top of that ink halftone.

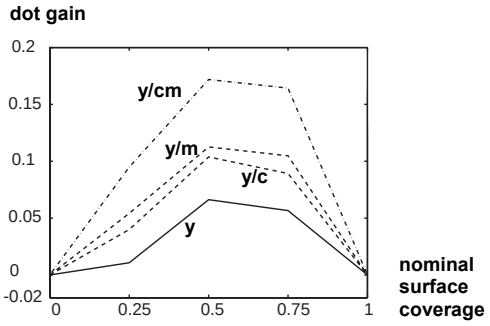

Figure 2. *The dot gain of a clustered yellow ink halftone dot, printed in offset at 150lpi, alone (y), superposed with cyan (y/c), superposed with magenta (y/m) and superposed with cyan and magenta (y/cm).*

Reflection prediction models need therefore to account for both the interaction of light with the print (yielding a so-called *optical dot gain*) and for the spreading of ink halftones depending on the superposition conditions (yielding the so-called *mechanical dot gain*).

Radiometry and optics

In order to establish physically-based spectral prediction models and to calibrate these models with measured reflectance spectra, it is necessary to introduce a few basic definitions and rules from the fields of radiometry and geometric optics. The presentation is inspired from the radiometric approach developed by Hebert & Hersch [1].

Keynote Talk, Proc. IS&T Third European Conference on Color in Graphics, Imaging and Vision (CGIV), Leeds, June 2006, pp. 1-7

A *radiant flux* $\Phi(\lambda)$ expresses a wavelength dependent radiation. An irradiance $E(\lambda)$ expresses a radiant flux per unit area, passing through or emerging from a surface element

$$E(\lambda) = \mathrm{d}\Phi(\lambda)/ds. \quad (1)$$

A *radiance* $L(\lambda)$ is the radiant flux per unit projected area and per solid angle that is incident on, passing through or emerging from a point in a specified surface :

$$L(\lambda) = \frac{d\Phi(\lambda)}{ds \cdot \cos\theta \cdot d\omega} \quad (2)$$

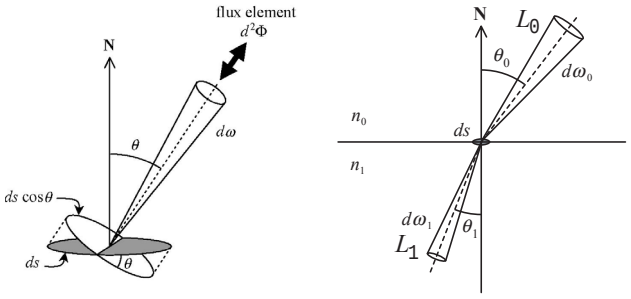

(a) **(b)**

Figure 3. *(a) A radiance L is a flux element per solid angle dω per projected surface element ds cosθ ; (b) a radiance L_1 refracted across an interface into a radiance L_0*

A *Lambertian reflector* is a perfect diffuser reflecting light at a constant radiance in all directions, independently of the orientation of the incident light. An incident irradiance E_i is reflected by a Lambert reflector as a radiance $L=\rho E_i/\pi$, where ρ expresses the reflectance of the reflector.

At an *interface* between two media of different indices of refraction, Snell's law and Fresnel's formulae apply. The incident light is reflected and refracted. Light incident from medium 0 (index of refraction n_0) at an angle of θ_0 is partly reflected at the same angle and partly refracted into medium 1 (index of refraction n_1), along angle θ_1. Snell's law states that

$$n_0 \sin\theta_0 = n_1 \sin\theta_1 \quad (3)$$

The Fresnel formulae give the portion of the incident light that is transmitted (refracted) from the air into the paper (or vice-versa)

$$r_{n_0/n_1}(\theta_0) = \frac{1}{2}\left[\frac{\tan^2(\theta_0-\theta_1)}{\tan^2(\theta_0+\theta_1)} + \frac{\sin^2(\theta_0-\theta_1)}{\sin^2(\theta_0+\theta_1)}\right] \quad (4)$$

Thanks to the Fresnel formulae, we may also compute how much light is internally reflected at the print-air interface. The paper bulk can be modeled as a Lambert reflector (Fig. 4), i.e. as a device emitting a constant radiance $L=\rho E_{1in}/\pi$, where ρ characterizes the reflectance of the paper bulk. At each angular orientation θ, an irradiance element

$$\mathrm{d}E = L\cos\theta\,\mathrm{d}\omega = \rho\,(E_{1in}/\pi)\cos\theta\,\mathrm{d}\omega \quad (5)$$

is emitted by the paper bulk (Lambertian reflector) within an infinitesimal solid angle $\mathrm{d}\omega$.

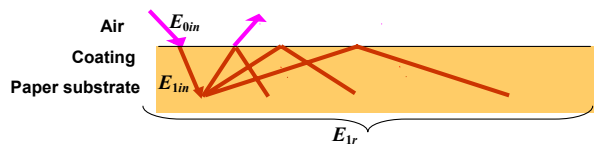

Figure 4*. Irradiance elements reflected by the paper bulk.*

A fraction $R_{10}(\theta)$, given by the Fresnel formulae, of each irradiance element of orientation θ located within an elementary solid angle $\mathrm{d}\omega$ reaching the print air interface is reflected. One obtains the total amount of reflected irradiance by integrating the irradiance elements individually reflected at the print-air interface over the whole hemisphere.

$$E_{1r} = \int \rho\frac{E_{1in}}{\pi}\cdot R_{10}(\theta)\cos\theta\cdot d\omega$$

$$= \int_0^{2\pi}\int_0^{\pi/2} \rho\frac{E_{1in}}{\pi}R_{10}(\theta)\cos\theta\sin\theta\,d\theta\,d\varphi$$

$$= \rho\ E_{1in}\int_0^{\pi/2} R_{10}(\theta)\sin 2\theta\ d\theta \quad (6)$$

By dividing the reflected total irradiance E_{1r} by the irradiance ρE_{1in} incident on the print-air interface, we obtain the average reflection r_i of Lambertian light at the print-air interface

$$r_i = \int_0^{\pi/2} R_{10}(\theta)\sin 2\theta\ d\theta \quad (7)$$

The amount of emerging irradiance E_{1t} crossing the print-air interface is simply $E_{1t} = (1-r_i)\,\rho\,E_{1in}$ due to the conservation of energy. The total irradiance emerging from a print can be measured with an integrated sphere. However, most spectrophotometers do not measure an irradiance, but rather a radiance, at a certain angular orientation, e.g. at 0 degrees.

Let us characterize the radiance emerging from an interface. We consider a radiance $L_{1t}(\theta_1)$ emitted by the paper bulk incident on a surface element *ds* of the interface. It represents an irradiance element within a conic solid angle $\mathrm{d}\omega_1$ (Fig. 3b) Due to Snell's rule, that irradiance element will exit at an angle θ_0, under the conic solid angle $\mathrm{d}\omega_0$.

Clearly, due to Snell's law, the cone aperture will be different in medium 0 from the one in medium 1 (Fig. 3b). Thanks to geometric considerations, by expressing solid angles $\mathrm{d}\omega_0$ and $\mathrm{d}\omega_1$ as a function of angle θ_1 and making use of Snell's law, one may verify the validity of the equation

$$\frac{ds\cos\theta_0 d\omega_0}{ds\cos\theta_1 d\omega_1} = \left(\frac{n_1}{n_0}\right)^2 \quad (8)$$

which expresses the ratio of the solid angle multiplied by the projected surface between medium 0 and medium 1. Since the element of irradiance emerging from the interface is the incident element of irradiance attenuated by $(1-R_{10}(\theta_1))$, we have

$$L_0\cos\theta_0\,\mathrm{d}\omega_0 = (1-R_{10}(\theta_1))\,L_1\cos\theta_1\,\mathrm{d}\omega_1 \quad (9)$$

The emerging radiance L_0 is therefore

$$L_0 = (1-R_{10}(\theta_1))\,(n_0/n_1)^2\,L_1 \quad (10)$$

Physically based spectral reflection model

Among the classical spectral prediction models, the Clapper-Yule model [2] is the only physically based model for halftone prints accounting for multiple internal reflectances at the print-air interface.

We express the reflectance *R* of a print as the ratio between the emerging irradiance E_{out} and the incident irradiance E_{in}.

$$R = E_{out}/E_{in} \quad (11)$$

The reflectance represents therefore the attenuation of the incident irradiance. It can be divided into an *input transmittance*

T_{in} representing the attenuation of the incident light entering the paper bulk, an *internal reflection* $R_{internal}$ representing the attenuation of light due to multiple reflections between the paper bulk and the print-air interface and an *exit transmittance* T_{out} representing the attenuation of light emerging from the print:

$$R = T_{in}\, T_{out}\, R_{internal} \tag{12}$$

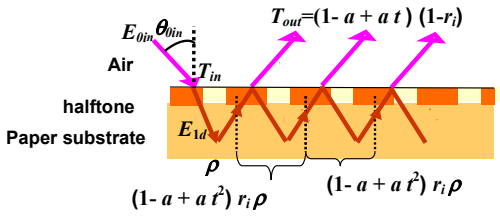

Figure 5. *Transmittance at the air-print interface, reflection within the substrate and internal reflections at the interface between the print and the air.*

With the notations shown in Fig. 5, the irradiance incident at angle θ penetrating both the interface and the halftone ink layer of dot surface coverage a is

$$E_{1d} = T_{01}(\theta_{0in})\,(1-a+a\,t)\,E_{0in} \tag{13}$$

Part a of the incident light having crossed the interface is attenuated by the ink transmittance t and part $(1-a)$ is not attenuated. The incident light reaching the paper bulk is therefore attenuated by

$$T_{in} = E_{1d} / E_{0in} = T_{01}(\theta_{0in})\,(1-a+a\,t) \tag{14}$$

The attenuation of light within the paper bulk yielding the internal reflectance of the print is determined by a first reflectance ρ within the paper bulk and successive internal reflections induced by one transversal of the halftone ink layer, by one internal reflection at the print-air interface, by a second traversal through the halftone ink layer and by one reflection from the paper bulk. One internal reflection cycle yields the attenuation $(1-a+a\,t^2)\,r_i\,\rho$. The irradiance E_{1up} ready to emerge from the print is the sum of all irradiance components reflected from the paper bulk. We obtain for the internal reflection

$$\begin{aligned} R_{internal} &= E_{1up} / E_{1d} \\ &= \rho\,(1+(1-a+a\,t^2)r_i\rho + ((1-a+a\,t^2)r_i\rho)^2 + ((1-a+at^2)r_i\rho)^3 + \ldots) \\ &= \rho\frac{1}{1-(1-a+a\cdot t^2)r_i\rho} \end{aligned} \tag{15}$$

The attenuation of the irradiance emerging from the print is simply the attenuation of the halftone ink layer $(1-a+a\,t)$ and the attenuation due to the interface transmittance $(1-r_i)$ when exiting from the print.

$$T_{out} = (1-a+a\,t)\,(1-r_i) \tag{16}$$

Finally, we obtain according to (12) for the global reflectance

$$R(\lambda) = \frac{T_{01}(\theta_{0in})\,(1-r_i)\,(1-a+a\cdot t)^2\,\rho}{1-(1-a+a\cdot t^2)r_i\rho} \tag{17}$$

This equation expresses the global spectral reflectance of a single ink halftone print. The transmittance of the ink $t(\lambda)$ and the intrinsic reflectance of the paper $\rho(\lambda)$ are wavelength dependent terms. $T_{01}(\theta_{0in})$ is the Fresnel transmittance for light incident on the print at angle θ_{0in}. The effective dot surface coverage is a. Reflectance $R(\lambda)$ represents the fraction of the incident irradiance emerging from the print. It has been first established in this form by Clapper and Yule in 1953 [2].

In the general case, it is not the reflectance but the reflectance factor that is measured, i.e. the reflectance relative to the reflectance of a perfectly white diffusing substrate (e.g. barium sulfate). When measuring the reflectances with an integrated sphere, besides the specular component, all emerging irradiance is captured. In that case, the reference reflectance of the perfectly white diffuse is one at all wavelengths and the measured reflectance factor of a printed sample is identical to its reflectance.

Often however, the measuring instrument is a photospectrometer having a 45°/0° geometry, i.e. emitting light at 45° and capturing the reflected radiance at 0°. In that case, we should not consider the emerging irradiance, but rather the emerging radiance. The irradiance traveling upwards from the paper bulk is E_{1up}. Since the paper bulk is assumed to be Lambertian, it emits the same radiance $L_{1up} = E_{1up}/\pi$ in all directions. Due to the attenuation by the halftone ink layer and to cone spreading (Eq. 10), the radiance emerging out of the print is

$$L_0 = (1-a+a\,t)\,(1-R_{10}(\theta_1))\,(n_0/n_1)^2\,L_{1up} \tag{18}$$

where θ_1 is the emerging angle within the print, corresponding, according to Snell's law, to the angle θ_{0out} of the radiance capturing measuring instrument. Since $(1-R_{10}(\theta_1)) = T_{10}(\theta_1) = T_{01}(\theta_{0out})$, the radiance emerging from the print is

$$L_0 = (1-a+a\,t)\,T_{01}(\theta_{0out}))\,(n_0/n_1)^2\,E_{1up}/\pi \tag{19}$$

The exit attenuation $T_{outR/Ir} = L_0/E_{1up}$ undergone by the irradiance emitted by the paper bulk when exiting the print as a radiance at orientation θ_{0out} is therefore

$$T_{outR/Ir} = (1/\pi)\,T_{01}(\theta_{0out}))\,(n_0/n_1)^2\,(1-a+a\,t) \tag{20}$$

Then, the global attenuation $R_{R/Ir}$ expressing the ratio of emerging radiance to the incident irradiance becomes

$$R_{R/Ir} = \frac{T_{01}(\theta_{0in})T_{01}(\theta_{0out})}{\pi}\left(\frac{n_0}{n_1}\right)^2\frac{(1-a+a\cdot t)^2\,\rho}{1-(1-a+a\cdot t^2)r_i\rho} \tag{21}$$

The corresponding reflectance factor R_{fac}, measured by the radiance detector, is the print's global attenuation $R_{R/Ir}$ divided by the corresponding attenuation of the perfectly white diffuser used to calibrate the instrument, i.e. by $L_{instr}/E_{in} = (1/\pi)$. We obtain for the spectral reflection factor

$$R_{fac} = T_{01}(\theta_{0in})T_{01}(\theta_{0out})\left(\frac{n_0}{n_1}\right)^2\frac{(1-a+a\cdot t)^2\,\rho}{1-(1-a+a\cdot t^2)r_i\rho} \tag{22}$$

The reflection factor measured with a radiance capturing device distinguishes itself from the reflection factor measured with an integrated sphere by having in its equation the factor $T_{01}(\theta_{0out})\,(n_0/n_1)^2$ instead of $(1-r_i)$. Luckily, when measuring at a 45°/0° geometry, the two factors induce reflectance differences of less than 2.5%. By abuse of language, the measured reflection factor is often considered to represent the print's reflectance [3].

The previous equations are easily extended to multi ink halftone prints, by replacing the expression $(1-a+a\,t)$ with the sum of the colorant transmittances t_i, weighted by their corresponding surface coverages a_i, i.e. by $\Sigma(a_i\,t_i)$ and by replacing the expression $(1-a+a\,t^2)$ with the expression $\Sigma(a_i\,t_i^2)$, where the transmittance of the white colorant is simply 1. See the next section regarding the computation of the colorant surface coverages.

Ink and colorant surface coverages

When printing with multiple, at least partly transparent inks, the superposition of two or more inks yields new colorants (Fig. 6). Therefore, with the inks cyan, magenta and yellow, one may obtain by printing superposed dots the colorants cyan, magenta, yellow, red (superposition of magenta and yellow), green (superposition of yellow and cyan), blue (superposition of magenta and cyan) and black (superposition of cyan, magenta and yellow). In many printing devices, the ink layers are printed independently one from another (e.g. the classical mutually rotated screens). Within a single halftone ink layer, the probability that light hits at a position (x,y) an inked dot is equal to the surface coverage of that ink in the region within which the position (x,y) is located. When two layers with respective surface coverages c_1 and c_2 are printed independently one from another, the probability that light hits at a given position both an ink dot from the first layer and an ink dot from the second layer is equal to the multiplication of their respective surface coverages, i.e. $c_1 c_2$. Accordingly, in the case of surface coverages of cyan c, magenta m and yellow y, the so-called Demichel equations yield the respective surface coverages of the colorants a_i as a function of the surface coverages c, m, and y of the inks:

white: $a_w = (1 - c)\,(1 - m)\,(1 - y)$
cyan: $a_c = c\,(1 - m)\,(1 - y)$
magenta: $a_m = (1 - c)\,m\,(1 - y)$
yellow: $a_y = (1 - c)\,(1 - m)\,y$ (23)
red: $a_r = (1 - c)\,m\,y$
green: $a_g = c\,(1 - m)\,y$
blue: $a_b = c\,m\,(1 - y)$
black: $a_k = c\,m\,y$

Figure 6. *Colorants cyan, magenta and yellow generated by single inks printed on paper, colorants red, green and blue generated by the superposition of two inks and colorant black generated by the superposition of the three inks.*

Other color halftoning algorithms (e.g. dot-on-dot) may induce other relationships between ink dot surface coverages and colorant surface coverages.

Neugebauer spectral prediction models

The spectral Neugebauer model [4] [5] predicts the reflection spectrum $R(\lambda)$ of a printed color halftone patch as the sum of the reflection spectra $R_i(\lambda)$ of its individual colorants weighted by their surface coverages a_i

$$R(\lambda) = \sum a_i\, R_i(\lambda) \qquad (24)$$

Since the Neugebauer model neither takes explicitly into account the lateral propagation of light within the paper bulk nor the internal reflections (Fresnel reflections) at the print-air interface, its predictions are not accurate. Yule and Nielsen [6] modeled the non-linear relationship between reflection values of colorants and reflection values of single ink halftones by an empirical power function, with fitted exponent n. Viggiano [5] applied the Yule-Nielsen relationship to the spectral Neugebauer equations, yielding the *Yule-Nielsen modified Spectral Neugebauer model :*

$$R = \left(\sum_i a_i \cdot R_i^{1/n} \right)^n \qquad (25)$$

This Yule-Nielsen modified Spectral Neugebauer model (short: Yule-Nielsen model) is widely used for the characterization of printers [7] [8] [9] [10]. It plays a significant role for characterizing printing devices and building color management systems.

Ink spreading models

Most optimization approaches for computing the effective surface coverages of ink dots as a function of the nominal surface coverages assume that the dot gain of an ink halftone remains constant in different superposition conditions [7] [10]. However, as is shown in Fig. 2, this is generally not the case. There has also been an attempt to combine in a multiplicative manner the ink spreading factors of successive halftone layers [9]. This approach seems to make sense for offset on coated paper, but not for other technologies, such as thermal transfer, where an ink dot printed in superposition with a second solid ink has a smaller effective surface coverage than the same ink dot printed alone on paper. A recent ink spreading model was proposed for ink-jet printing which relies on the geometry of configurations of hexagonal dot overlaps and which computes ink spreading by spatially varying the ink dot thickness profile [11]. However, this ink spreading model is not applicable to classical spectral prediction models (Clapper-Yule, Yule-Nielsen) which assume that the ink thickness is constant, independently of the dot size.

Let us describe a recently developed ink spreading model which was successfully applied both to the Clapper-Yule [3] and to the Yule-Nielsen [12] reflectance prediction models. This general-purpose ink spreading model relies on the assumption that, when a halftone layer is printed either beneath or on top of a solid layer, its effective surface coverage is modified.

We calibrate the ink spreading model by creating separate ink spreading functions mapping nominal surface coverages to (a) the effective surface coverages of single ink halftones, (b) effective surface coverages of single ink halftones superposed with one solid ink (c) effective surface coverages of single ink halftones superposed with two solid inks and possibly (d) effective surface coverages of single ink halftones superposed with three solid inks.

After establishing the ink spreading functions (calibration), we obtain the effective dot surface coverages (c',m',y') of a color halftone patch as a function of its nominal surface coverages (c,m,y) by weighting the contributions of the different ink spreading functions according to their corresponding relative colorant surfaces.

At calibration time, an ink spreading function is created for every superposition condition by fitting effective surface coverages (e.g. at 25%, 50% and 75% nominal coverages) of the halftone ink which minimize the square distances between the reflection spectrum vectors predicted according to the chosen spectral prediction model (Clapper-Yule, Yule-Nielsen, etc.) and the measured reflection spectrum vectors. This yields for each nominal surface coverage an effective (fitted) surface coverage. For each superposition condition, by linear interpolation between the so obtained effective surface coverages, we create the corresponding ink spreading function. Ink spreading functions are similar to tone reproduction curves: they map

nominal to effective surface coverages of each ink halftone, each one at a specific ink superposition condition.

Let us consider halftone patches comprising cyan, magenta and yellow inks printed at respective nominal dot surface coverages c, m and y. The ink spreading functions mapping nominal surface coverages to effective surface coverages for single ink halftones printed on paper are $f_c(c)$, $f_m(m)$ and $f_y(y)$. The ink spreading functions mapping nominal coverages of an ink to effective coverages of that ink, for single ink halftones superposed with a second solid ink and for single ink halftones superposed with two solid inks are:

$f_{c/m}(c)$: *cyan* of coverage c superposed with solid ink *magenta*,
$f_{c/y}(c)$: *cyan* of coverage c superposed with solid ink *yellow*,
$f_{m/c}(m)$: *magenta* of coverage m superposed with solid ink *cyan*,
$f_{m/y}(m)$: *magenta* of coverage m superposed with solid *yellow*,
$y_{y/c}(y)$: *yellow* of coverage y superposed with solid ink *cyan*,
$y_{y/m}(y)$: *yellow* of coverage y superposed with solid *magenta*,
$f_{c/my}(c)$: *cyan* of coverage c superposed with solid inks *magenta* and *yellow*,
$f_{m/cy}(m)$: *magenta* of coverage m superposed with solid inks *cyan* and *yellow*:
$f_{y/cm}(y)$: *yellow* of coverage y superposed with solid inks *cyan* and *magenta*.

In the case of three inks, these 12 functions may for example be obtained by fitting 36 patches, i.e. 3 patches (25%, 50% and 75% nominal coverages) per ink spreading function.

Figure 2 gives an example of dot gains obtained by fitting effective surface coverages according to the Yule-Nielsen model, for step wedges printed alone, for step wedges printed in superposition with one solid ink and for step wedges printed in superposition with two solid inks. Yellow halftones alone (y) have a smaller dot gain than yellow halftones printed in superposition with solid magenta (y/m) or solid cyan (y/c). Yellow halftones printed in superposition of solid cyan and magenta (y/cm) have the largest dot gain. In order to obtain the effective surface coverages c_1', c_2' and c_3' of a color halftone patch, it is necessary, for each ink i_k, to weight the contributions of the corresponding mapping functions f_k, $f_{k/l}$, $f_{k/m}$, and $f_{k/lm}$. The weights depend on the effective coverages of the considered ink alone, of the considered ink in superposition with a second ink and of the considered ink in superposition with the two other inks. The relative weights of the superposition conditions contributing to a given ink halftone are the surface coverage ratios of their contributing colorants. For example, within a halftone patch printed with ink *cyan* of coverage *c,* the proportion of ink *cyan* printed on paper white only is (1- m') (1- y'). The proportion of ink *cyan* printed in superposition with solid ink *magenta* only is m' (1-y'). The proportion of ink *cyan* printed on top of solid ink *yellow* only is (1-m') c_3'. Finally, the proportion of ink *cyan* printed in superposition with solid inks *magenta* and *yellow* is m'. y'. We obtain the following system of equations:

$$
\begin{aligned}
c' &= f_c(c)\,(1-m')\,(1-y') \\
&\quad + f_{c/m}(c)\,m'\,(1-y') + f_{c/y}(c)(1-m')\,y' + f_{c/my}(c)\,m'\,y' \\
m' &= f_m(m)\,(1-c')\,(1-y') + f_{m/c}(m)\,c'\,(1-y') \\
&\quad + f_{m/y}(m)\,(1-c')\,y' + f_{m/cy}(m)\,c'\,y' \qquad (26) \\
y' &= f_y(y)\,(1-c')\,(1-m') + f_{y/c}(y)\,c'\,(1-m') \\
&\quad + f_{y/m}(y)\,(1-c')\,m' + f_{y/cm}(y)\,c'\,m'
\end{aligned}
$$

In order to compute the effective surface coverages c', m' and y' , this system of equations can be solved iteratively: one starts by setting initial values of c', m' and y' equal to the respective nominal coverages c, m and y. After one iteration, one obtains new values for c', m' and y'. These new values are used for the next iteration. After a few iterations, the system stabilizes and the resulting surface coverages c', m' and y' are the effective ink dot surface coverages.

For most spectral reflectance prediction models, one needs however the effective colorant surface coverages. In the case of three independently printed ink layers, the effective colorant coverages a_1', a_2', .. a_8' are obtained from the effective coverages c', m' and y' of the inks according to the Demichel equations (Eqs. 23)**.** The whole spectral reflection prediction framework accounting for ink spreading in all superposition conditions is illustrated in Fig. 7.

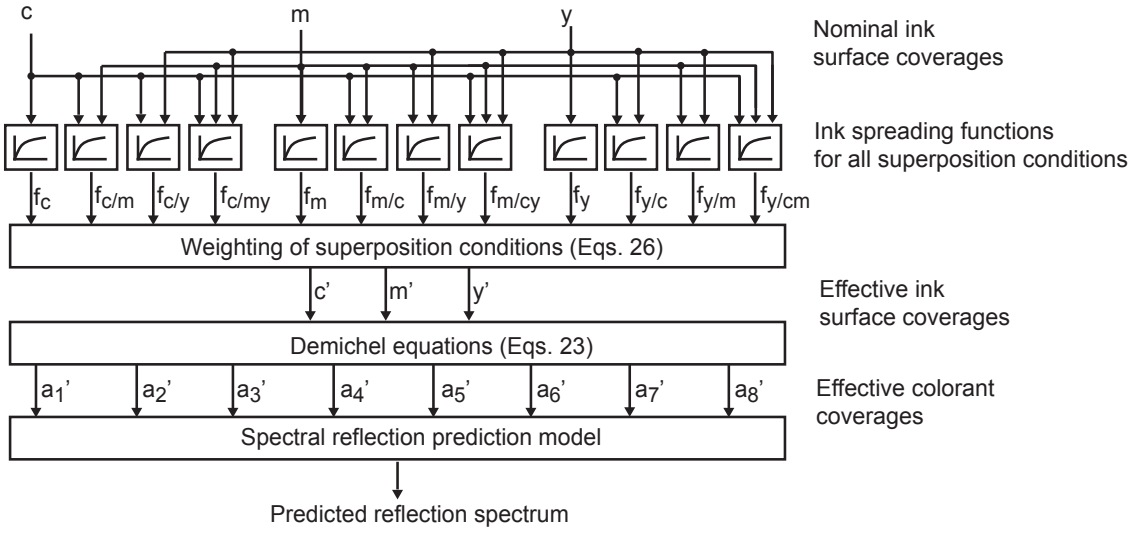

Figure 7. *Spectral prediction framework comprising both the spectral prediction and the ink spreading model*

Remaining challenges

The presented physically based spectral prediction model (Clapper-Yule) makes a number of assumptions which are not always present in halftone prints.

1. For light emerging from the paper bulk, the probability of traversing a given colorant is equal to that colorant's effective surface coverage. Therefore the model makes the assumption that lateral propagation of light is important in respect to the screen period. Rogers [13] proposes an extension of the Clapper-Yule model which is also valid for relatively small screen periods. However, further work is needed to develop this approach towards a full blown model usable in practice. A more empirical approach relying on a weighted average between the Clapper-Yule model and an extension of the spectral Neugebauer model accounting for multiple internal reflections provides good prediction results also at low screen frequencies [3].

2. Printed ink dots are assumed to have a uniform thickness. However, as is known from ink-jet printing, the thickness profile of a single dot may exhibit significant variations, e.g. between the exterior and the interior of the dot. Further research is needed to account for variable dot thickness profiles.

3. There has been a considerable body of work which modeled lateral propagation of light within the paper bulk by a point spread function without accounting explicitly for multiple internal reflections [14] [15] [16] [17]. Various phenomena were modeled, such as ink penetration within the paper bulk [17] [18], ink spreading [19] and non-uniform ink dot density [20]. Since the internal reflections are not explicitly modeled, the point spread function represents the effects of both the lateral propagation of light and the multiple internal reflections. Recently, these approaches have been refined by associating to the point spread function only the lateral propagation of light and by incorporating the point spread function into a multiple internal reflection model [13] [21].

4. In the explanations above, we assume that the paper and the inks are non-fluorescent. However, fluorescence models have been proposed [22] [23] [24]. Their integration into a full spectral prediction framework is not an easy task.

5. Both the Clapper-Yule and the Yule-Nielsen spectral prediction models, combined with the ink spreading model, enable making accurate spectral reflectance predictions. However, the Yule-Nielsen model is not restricted to high screen frequencies. Although the Yule-Nielsen model has been analyzed in the past [14], further research is needed in order to understand why it provides accurate results for different print technologies, for different halftoning algorithms and at different screen frequencies.

6. Printing with special inks such as opaque or partially opaque inks (i.e. scattering inks) introduces new problems. It is not yet know if the Clapper-Yule and Yule-Nielsen models relying on effective colorant surface coverages remain valid, since part of the light is scattered from within the ink layer without reaching the paper bulk.

Conclusions

Thanks to the newly developed ink spreading model, both the classical Clapper-Yule and Yule-Nielsen modified spectral prediction models are capable of providing accurate reflectance predictions. Thanks to these models, we get a better understanding of the complex interactions between light, ink halftones and paper. However, further research is needed in order to verify that the computed ink dot surface coverages indeed correspond to the real printed ink dot surface coverages and that the computed ink transmittances correspond to the real ink transmittances. Nevertheless, since these models provide accurate predictions, they may also be used in order to verify that the same paper-ink combinations are used in successive print jobs. Further developments relying on these spectral prediction models may possibly allow keeping printer parameters such as ink thickness or dot gain constant over long printing periods.

Acknowledgements

The authors thank the Swiss National Science Foundation for its support (grant no. 200020-105119/1) and Thomas Bugnon for having corrected the manuscript. They also thank previous members of the research team who contributed to the project (P. Emmel, F. Collaud, F. Crété).

References

[1] M. Hebert, R.D. Hersch, Classical Print Reflection Models, a Radiometric Approach, Journal of Imaging Science and Technology, Vol. 48, No. 4, 363-374 (2004).

[2] F.R. Clapper, J.A.C Yule, The effect of multiple internal reflections on the densities of halftone prints on paper, J. of the Optical Society of America, Vol. 43, 600-603 (1953)

[3] R.D. Hersch, P. Emmel, F. Crété, F. Collaud, Spectral reflection and dot surface prediction models for color halftone prints, J. of Electronic Imaging, Vol. 14, No. 3, August 2005, 33001-12

[4] H.E.J. Neugebauer, Die theoretischen Grundlagen des Mehrfarbendrucks. *Zeitschrift fuer wissenschaftliche Photographie,* Vol. 36, 36-73, (1937), reprinted in *Neugebauer Seminar on Color Reproduction,* SPIE Vol-1184,194-202 (1989)

[5] J.A.S Viggiano, Modeling the Color of Multi-Colored Halftones, Proc. TAGA, 44-62 (1990)

[6] J.A.C. Yule, W.J. Nielsen, The penetration of light into paper and its effect on halftone reproductions, Proc. *TAGA*, Vol. 3, 65-76 (1951),

[7] R. Balasubramanian, Optimization of the spectral Neugebauer model for printer characterization, Journal of Electronic Imaging, Vol. 8, No. 2, 156-166 (1999)

[8] K. Iino, R.S. Berns, Building color management modules using linear optimization I. Desktop, Journal of Imaging Science and Technology, Vol. 42, No. 1, 79-94 (1998)

[9] K. Iino, R.S. Berns, Building color management modules using linear optimization II. Prepress system for offset printing, Journal of Imaging Science and Technology, Vol. 42, No. 2, 99-114 (1998)

[10] M. Xia, E. Saber, G. Sharma, M. Tekalp, End to end color printer calibration by total least squares regression, IEEE

Trans. On Image Processing, Vol. 8, No. 5, May 1999, 700-716

[11] P. Emmel, R.D. Hersch, Modeling ink spreading for color prediction, Journal of Imaging Science and Technology, Vol. 46, No. 3, 237-246, (2002)

[12] R.D. Hersch, F. Crété, Improving the Yule-Nielsen modified spectral Neugebauer model by dot surface coverages depending on the ink superposition conditions, IS&T/SPIE Electronic Imaging Symposium, Conf. Imaging X: Processing, Hardcopy and Applications, Jan. 05, SPIE Vol. 5667, 434-445

[13] G. Rogers, A Generalized Clapper-Yule Model of Halftone Reflectance. *Journal of Color Research and Application,* Vol. 25, No. 6, 402-407 (2000)

[14] F.R. Ruckdeschel, O.G. Hauser, Yule-Nielsen in printing: a physical analysis, Applied Optics, Vol. 17, No. 21, 3376-3383 (1978)

[15] G. Rogers, Optical Dot Gain: Lateral Scattering Probabilities, Journal of Imaging Science and Technology, Vol. 42, No. 4, 341-345, (1998)

[16] J. S. Arney, A Probability Description of the Yule-Nielsen Effect I, Journal of Imaging Science and Technology, Vol. 41, No. 6, 633-636 (1997)

[17] L. Yang, R. Lenz, B. Kruse, Light scattering and ink penetration effects on tone reproduction, Journal of the Optical Society of America A, Vol. 18, No. 2, 360-366 (2001)

[18] L. Yang, B. Kruse, Ink penetration and its effects on printing, Electronic Imaging Symposium, Conf. Color Imaging: Device-Independent Color, Color Hardcopy and Graphic Arts V, San Jose, CA, Jan, 2000, SPIE Vol. 3963, 365-375

[19] J.S. Arney and M. Alber, Optical Effects of Ink Spread and Penetration on Halftones Printed by Thermal Ink Jet, Journal of Imaging Science and Technology, vol. 42, no. 4, 331-334 (1998)

[20] J.S. Arney, P. Mehta, P. G. Anderson, A Continuous Tone Model of Halftones, Journal of Imaging Science and Technology, Vol. 48, No. 1, 45-49 (2004)

[21] P. Emmel, R.D. Hersch, A Unified Model for Color Prediction of Halftoned Prints, Journal of Imaging Science and Technology, Vol. 44, No. 4, 351-359 (2000)

[22] P. Emmel, R.D. Hersch, Spectral Colour Prediction Model for a Transparent Fluorescent Ink on Paper, Proc. IS&T/SID 6th Color Imaging Conference: Color Science, Systems and Applications, Nov,1998, Scottsdale, AZ, 116-12

[23] G. L. Rogers, Spectral model of a fluorescent ink halftone, J. Opt. Soc. Am. A, Vol. 17, No. 11, Nov. 2000, 1975-1981

[24] Li Yang, Spectral Model of Halftone on a Fluorescent Substrate, J. of Imaging Science and Technology, March/April 2005, vol. 49, no. 2, 179-184